Mapping Backbone Dynamics in Solution with Site-Directed Spin Labeling: GCN4−58 bZip Free and Bound to DNA†

Linda Columbus and Wayne L. Hubbell*

Jules Stein Eye Institute and Department of Chemistry and Biochemistry, University of California, Los Angeles, California 90095-7008

Received January 29, 2004; Revised Manuscript Received April 9, 2004

ABSTRACT: In site-directed spin labeling, a nitroxide-containing side chain is introduced at selected sites in a protein. The EPR spectrum of the labeled protein encodes information about the motion of the nitroxide on the nanosecond time scale, which has contributions from the rotary diffusion of the protein, from internal motions in the side chain, and from backbone fluctuations. In the simplest model for the motion of noninteracting (surface) side chains, the contribution from the internal motion is sequence independent, as is that from protein rotary diffusion. Hence, differences in backbone motions should be revealed by comparing the sequence-dependent motions of nitroxides at structurally homologous sites. To examine this model, nitroxide side chains were introduced, one at a time, along the GCN4−58 bZip sequence, for which NMR ^{15}N relaxation experiments have identified a striking gradient of backbone mobility along the DNA-binding region [Bracken et al. (1999) *J. Mol. Biol. 285*, 2133]. Spectral simulation techniques and a simple line width measure were used to extract dynamical parameters from the EPR spectra, and the results reveal a mobility gradient similar to that observed in NMR relaxation, indicating that side chain motions mirror backbone motions. In addition, the sequence-dependent side chain dynamics were analyzed in the DNA/protein complex, which has not been previously investigated by NMR relaxation methods. As anticipated, the backbone motions are damped in the DNA-bound state, although a gradient of motion persists with residues at the DNA-binding site being the most highly ordered, similar to those of helices on globular proteins.

Proteins are inherently dynamic structures. On the fast pico- to nanosecond time scale, atoms of the backbone and side chains collectively fluctuate about their average positions. On a microsecond or longer time scale, proteins may switch between discrete conformational substates. Both dynamic modes can be related to function. For example, amplitudes of backbone fluctuations often vary dramatically throughout the structure, and flexible sequences have been found to be involved in protein−protein (*1*−*3*) or protein−ligand interactions (*4*) and in conferring thermodynamic stability to a structure (*5*, *6*). In addition, backbone fluctuations and side chain motions may be essential "lubricants" for the interconversions between conformational substates (*7*). Conformational switching is recognized as a fundamental mechanism of protein function (*8*, *9*).

Due to the essential link between protein dynamics and function, there is great interest in experimental strategies to explore both conformational switching and fluctuations. NMR[1] relaxation techniques that monitor the reorientation of a labeled heavy atom−H bond vector (e.g., ^{15}N−H) have succeeded in describing the pico- to nanosecond backbone motions for small proteins in solution (*2*). When interpreted in terms of the Lipari−Szabo formalism, the data provide the frequency of bond motion as an effective correlation time, τ_e, and amplitude of motion, which is measured by the square of an order parameter (S^2). Obtaining similar dynamic information on large complexes and membrane proteins using NMR relaxation experiments remains challenging due to technical difficulties related to the size of the protein and sample limitations.

SDSL has emerged as a useful approach for the investigation of protein structure and conformational dynamics (*10*, *11*) and has the potential to provide direct information on backbone dynamics (*12*, *13*). SDSL utilizes site-directed mutagenesis to replace the residue of interest with a cysteine and all reactive native cysteine residues with a suitable substitute. The unique cysteine residue is then modified with a sulfhydryl-specific nitroxide reagent to introduce a paramagnetic side chain that is sensitive to the local environment. In most studies, the side chain designated R1(a) in Figure 1 has been employed.

The EPR spectrum of a spin-label probe encodes information about the dynamic modes of the nitroxide. Such information is of interest because the nitroxide motion reflects a variety of structural and dynamic features of the protein itself. These include Brownian rotary diffusion of the protein, backbone dynamics, segmental rigid body

† This work was supported by NIH Grants EY05216 and T32 EY07026, the Jules Stein Professor Endowment, and a grant from the Bruce Ford and Anne Smith Bundy Foundation.

* Corresponding author. Phone: (310) 206-8830. Fax: (310) 794-2144. E-mail: hubbellw@jsei.ucla.edu.

[1] Abbreviations: NMR, nuclear magnetic resonance; EPR, electron paramagnetic resonance; SDSL, site-directed spin labeling; DNA, deoxyribonucleic acid; MOMD, microscopic order macroscopic disorder; M_s, scaled mobility; IPTG, isopropyl β-D-thiogalactoside; EDTA, ethylenediaminetetraacetate; BME, β-mercaptoethanol; PMSF, phenylmethanesulfonyl fluoride; DTT, dithiothreitol; SDS, sodium dodecyl sulfate; T4L, T4 lysozyme; PDB, Protein Data Bank.

10.1021/bi0497906 CCC: $27.50
Published on Web 05/18/2004

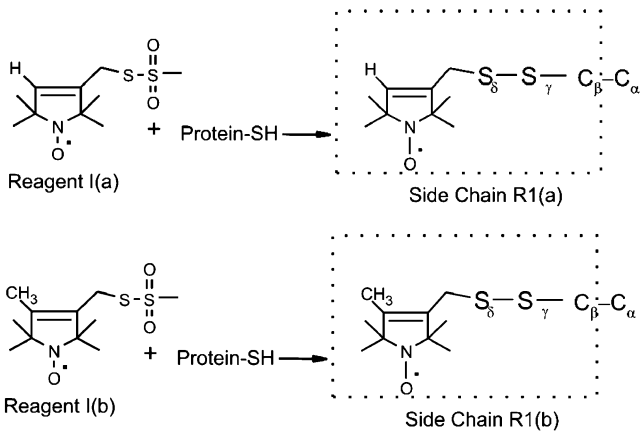

FIGURE 1: Reaction of spin-labeling reagents I(a) and I(b) to generate nitroxide side chains R1(a) and R1(b).

motions, and bond rotational isomerizations within the side chain, the latter being modulated by interactions of the side chain with its environment. One of the goals in the development of SDSL is to resolve these different contributions to the nitroxide motion and provide an experimental tool for the investigation of protein dynamics as well as protein structure. Achieving such a deconvolution from first principles requires knowledge of the inherent dynamic modes of the nitroxide side chain and how these modes are modulated by structural interactions. By correlating spectral simulations (*12*, *14*), variation of side chain structures (*12*, *15*), and crystal structures of spin-labeled proteins (*16*), significant progress has been made in this direction for the R1(a) side chain at a particularly simple site: the solvent-exposed surface of an α-helix.

At solvent-exposed sites on α-helices where the side chain has no interactions with neighboring residues, the distinctive EPR spectral line shapes can be accurately fit by the *m*icroscopic *o*rder *m*acroscopic *d*isorder (MOMD) model of Freed and co-workers with an order parameter (S_{20}) and effective correlation time (τ) that describe the diffusive motion of the nitroxide 2p orbital under the restraint of an ordering potential (*12*).

The structural origin of the ordering potential was elucidated by crystal structures of T4L containing the R1(a) side chain and appears to be an interaction of the S_δ atom with backbone atoms of the R1(a) amino acid (Figure 2A, dashed line) (*16*). This interaction constrains motions about the first two bonds (defined by dihedrals X_1 and X_2) and, together with the intrinsic barrier to rotation about the disulfide (X_3), leads to a first-approximation "X_4/X_5" model in which limited torsional oscillations about the two terminal bonds of the side chain largely determine the motion of the nitroxide ring (*12*). Limited torsional oscillations about X_4/X_5 give rise to a motion of the nitroxide 2p orbital in a cone that can be described by an order parameter and effective correlation time (*12*, *13*) (Figure 2B). Thus, the physical model accounts for the MOMD mathematical description of the EPR spectra.

An example spectrum of a noninteracting helix surface site, residue 72R1(a) in the long interdomain helix of T4L (*12*, *13*), and the corresponding MOMD fit is shown in Figure 2C. The well-resolved parallel ($A_{||}$) and perpendicular ($A_\perp$) hyperfine extrema in the spectrum (arrows in Figure 2C) are characteristic of an anisotropic motion with S_{20} greater than approximately 0.3. Residue T4L 72R1(a) is

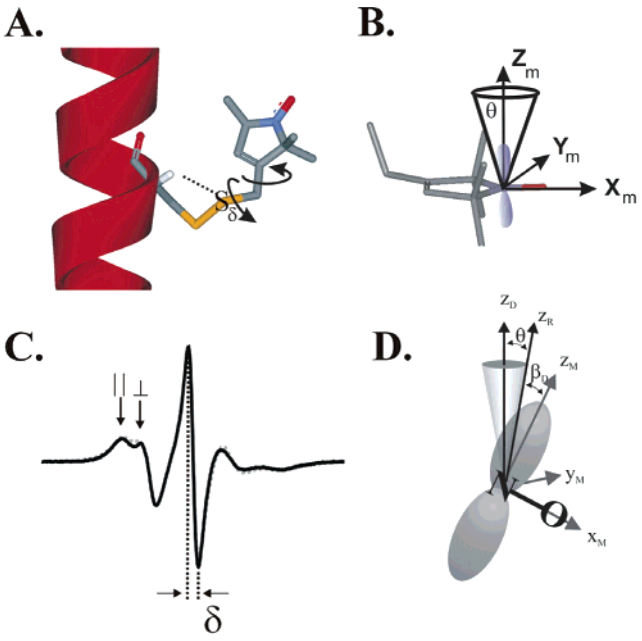

FIGURE 2: A model for the motion of the R1 side chain on α-helices. (A) A model of R1(a) on a solvent-exposed helix site. The dotted line represents the apparent interaction between S_δ and the hydrogen atom of C_α (*16*). The arrows indicate oscillations about dihedrals X_4 and X_5. (B) A model of R1(a) showing the motion of the nitroxide 2p orbital in a cone due to torsional oscillations about X_4 and X_5. (C) Experimental (black) and best-fit (gray dashed line) spectra for 72R1(a) of T4L. The fit was generated for the MOMD model using an order parameter $S_{20} = 0.47$ and $\tau = 2$ ns (*12*). The central line width is designated as δ. The resolved hyperfine components $A_{||}$ and $A_\perp$ are indicated by arrows. (D) Coordinate frames used in the MOMD model of nitroxide motion (see text).

particularly significant because it is in a helix that apparently has little backbone motion in the nanosecond regime (*12*, *13*). This being the case, S_{20} and τ values for R1(a) at this site are measures of the internal modes of the R1 side chain exclusively. Within the context of the X_4/X_5 model, the internal modes of R1 are independent of position along a helix, and variations of the dynamical parameters (S_{20} and τ) among structurally similar sites should reflect contributions from other dynamic modes, namely, backbone fluctuations. Such additional modes are expected to decrease τ and S_{20} relative to the T4L 72R1(a) reference site. A test of this simple model is a goal of the present work.

Although spectral simulations can be employed to model the side chain motion at each site studied, it is also desirable to have simple measures of nitroxide dynamics that can be used to analyze large-scale studies of protein dynamics with SDSL. Such measures include the inverse of the central resonance line width (δ, Figure 2C) (*15*) and a normalized version thereof (M_s) (*11*). In principle, these measures reflect both the rate and order (amplitude) of the nitroxide motion. For this reason, they have been referred to as measures of nitroxide "mobility", a qualitative descriptor of motion that implies both rate and order. In this work, the dependence of M_s on order (S_{20}) and correlation time (τ) is investigated using simulated spectra. For R1 motions on helices, it is found that M_s depends primarily on τ.

According to the model presented above, measures of side chain mobility, whether S_{20} and τ values extracted from spectral fitting procedures or the simple M_s, should vary along a sequence in proportion to backbone fluctuations in

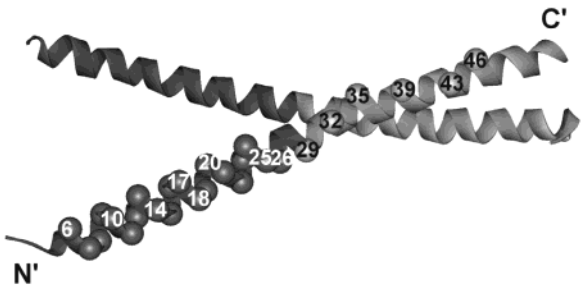

FIGURE 3: Ribbon model of GCN4−58. The ribbon of the basic DNA-binding region is colored dark gray, and the leucine zipper is in light gray. The sites at which spin-labeled side chains were introduced one at a time are indicated with spheres, and select sites are labeled.

the pico- to nanosecond time scale. To evaluate this idea, the site-dependent variation of the EPR spectra of nitroxide side chains R1(a) and R1(b) (shown in Figure 1) along the basic leucine zipper (bZip) of GCN4 was investigated. GCN4 bZip is a homodimeric motif in the DNA-binding transcription factor GCN4 (Figure 3). The GCN4 bZip motif investigated in the current study consists of the C-terminal 58 residues of GCN4 and will be designated GCN4−58 (*17*). The C-terminus of GCN4−58 (29−58) forms a coiled coil (leucine zipper), and the highly basic N-terminus forms the DNA-binding region. In the free state, the basic region is thought to exist as an ensemble of structures with helical propensities. GCN4−58 was selected for study with SDSL because previous NMR studies identified a striking gradient of backbone motion along the sequence corresponding to the DNA-binding region, while the motion throughout the leucine zipper was comparatively low and constant (*17*). The results presented below show that the distinctive pattern of motion is clearly revealed in the sequence dependence of dynamical parameters derived from the EPR data, validating the utility of SDSL for monitoring backbone motions in proteins less accessible to NMR.

The crystal structures of GCN4−58 bound to two different DNA recognition sites were previously determined (*18*, *19*), and in both structures the helix binds to the major groove of DNA. SDSL was further applied to characterize the dynamics of GCN4−58 bound to DNA, providing the first insight into the dynamic modes of the bound state. Although the backbone motions of GCN4−58 are damped in the complex, a gradient of backbone dynamics persists. Previous calculations of the conformational entropy change in the binding reaction have assumed that the helices of GCN4−58 in the bound state have equal rigidity to helices found in globular proteins (*20*), but this is apparently not the case.

MATERIALS AND METHODS

Preparation of Spin-Labeled GCN4−58 Mutants

Cloning, Expression, and Purification of GCN4−58 Mutants. GCN4−58 mutants containing single cysteine substitutions at consecutive sites 6−27 and 32, 35, 39, 43, and 46 (Figure 3) were generated using the QuikChange method (Stratagene, La Jolla, CA). The entire GCN4−58 gene of each cysteine mutant was sequenced by Davis Sequencing (Davis, CA). Mutant plasmids were transformed into *Escherichia coli* BL21(DE3). Cell cultures were grown to an OD $\approx$ 1.0, and protein expression was induced by adding IPTG (1 mM final concentration). The cells were harvested by centrifugation after 3 h of induction. The cell pellets were resuspended in a buffer (pH = 7.5) containing 50 mM KH_2PO_4, 0.3 M NaCl, 1 mM EDTA, 0.1% v/v BME, and 0.1% w/v PMSF and sonicated for 4 × 1 min in an ice bath (output 4, duty cycle 50% using a Branson Sonifier 250 and a standard disruption horn). The cell debris was pelleted by centrifugation at 27000*g* for 15 min. The supernatant was filtered (0.2 μm) and loaded onto a SP-Sepharose Hi-Trap column (Amersham Biosciences, Piscataway, NJ) equilibrated with a buffer (pH = 7.5) consisting of 50 mM Tris, 1 mM EDTA, and 1 mM DTT. GCN4−58 was eluted with a linear NaCl gradient (from 0 to 2.0 M NaCl). Protein purity was estimated at 95% using gel eletrophoresis with a 15% SDS Phast gel (Amersham Biosciences, Piscataway, NJ).

Spin Labeling of GCN4−58 Mutants. Immediately before spin labeling, the protein was exchanged into a suitable buffer (50 mM sodium acetate and 50 mM KCl at pH 6.0) using a Hi-Trap desalting column (Amersham Biosciences, Piscataway, NJ). The GCN4−58 mutants (typically $\approx$25 μM) were incubated with 1:1 molar ratio with the desired spin-labeling reagent. The reaction was allowed to proceed at room temperature for at least 1 h. The protein solutions were washed several times ($\approx$3 × 3 mL) through a Centricon filter (3 kDa cutoff) and concentrated to 200 μM using a Microcon filter concentrator (3 kDa cutoff). The spin-labeled mutants are designated by the residue number at which the nitroxide is introduced and the designation for the nitroxide side chain given in Figure 1. For example, 6R1(a) is a mutant with an R1(a) side chain at residue 6.

At some sites, spin-labeled side chains showed magnetic dipolar interactions in the homodimer. To record the spectrum of the noninteracting species, the labeled homodimer was mixed with Cys-less wild-type GCN4−58 at a ratio of 1:5. Sufficient subunit exchange to eliminate the interaction was observed within minutes of mixing the labeled and unlabeled protein.

DNA Binding to Spin-Labeled GCN4−58 Mutants

DNA substrate, AP-1 or 2AP-1 (Integrated DNA Technology, Santa Clara, CA), was added to spin-labeled protein at a molar ratio equal to or greater than 2:1. The AP-1 sequence contains a double-stranded pseudopalindromic sequence that GCN4−58 recognizes *in vivo*: 5′-GAGATGACTCATCTC-3′ and 3′-CTCTACTGAGTAGAG-5′. The 2AP-1 construct contains two AP-1 binding sequences separated by six base pairs: 5′-GAGATGACTCATCGCGAGATGACTCATCTC-3′ and 3′-CTCTACTGAGTAGCGCTCTACTGAGTAGAG-5′. In some cases, the DNA/protein complexes were added to 60% Ficoll 70 (w/v) at a ratio of 1:1 for a final Ficoll 70 concentration of 30%. For tethering the protein/DNA complex to streptavidin−agarose beads (Novagen, Madison, WI), one of the strands of AP-1 was biotinylated at the 5′ terminus (Integrated DNA Technology, Santa Clara, CA) and annealed to an unlabeled complementary strand. The DNA was added to the streptavidin−agarose beads with a molar ratio of 1.5:1 (DNA:streptavidin). The mixture was incubated at room temperature and shaken for 30 min. The mixture was centrifuged at 500*g* for 10 min and the supernatant carefully decanted. The beads were washed twice by adding GCN4−58 labeling buffer, incubating, centrifuging, and decanting the supernatant. The final sample was prepared by mixing

the DNA-bound beads with the spin-labeled protein with the DNA concentration 2-fold higher than that of the protein.

DNA binding of spin-labeled GCN4−58 was verified using a native polyacrylamide gel shift. Two microliters of the EPR sample was loaded onto a 12−25% gradient gel (Amersham Biosciences, Piscataway, NJ). Native buffer strips and reverse polarity electrodes were used to run the gel on a Phast system (Amersham Biosciences, Piscataway, NJ). The gel was stained and destained using standard methods. Migration of the DNA-bound protein is significantly different from the unbound state, allowing a qualitative assessment of DNA binding of the spin-labeled mutants of GCN4−58.

DNA binding by the spin-labeled protein was also verified by EPR spectral changes. In essentially all cases, DNA binding significantly altered the motion of the spin label, and the stoichiometry was determined to be 1:1 by titration of the effect with increasing concentrations of DNA. Binding constants cannot be quantitatively determined using this method because the minimum detectable concentration of labeled protein is approximately 1 μM, whereas the DNA-binding constants are in the nanomolar range (*21*, *22*).

EPR of Spin-Labeled GCN4−58 Mutants

EPR Measurements. EPR spectra were recorded on a Varian E−109 spectrometer fitted with a two-loop one-gap resonator (*23*). Protein samples of 5 μL ($\approx$200 μM) were loaded in Pyrex capillaries (0.84 mm o.d. x 0.6 mm i.d.) sealed on one end. All spectra were acquired using a 2 mW incident microwave power. The modulation amplitude at 100 kHz was optimized for each spectrum to avoid spectral distortion. All spectra were normalized to the same area.

The inverse of the central resonance line width (δ; Figure 2C) is a semiquantitative measurement of the mobility of the nitroxide side chain. For convenience, a normalized central line width measure, M_s, is employed:

$$M_s = \frac{\delta_{exp}^{-1} - \delta_i^{-1}}{\delta_m^{-1} - \delta_i^{-1}}$$

where δ_{exp} is the central line width of R1 at the site of interest and δ_i and δ_m are the corresponding values at the most immobilized and mobile site observed in a protein under conditions where rotational diffusion of the protein as a whole does not contribute to the line width. This measure has the advantage of simplicity in that it ranges from 0 to 1. The parameters δ_i and δ_m are somewhat arbitrary and subject to revision, and δ_i depends to some extent on local polarity in the protein. However, relative values are of primary interest in analyzing a database, and these are not serious disadvantages. In the present study, the value of δ_m is set at 2.1 G, corresponding to R1 near the end of the disordered 18-residue C-terminal sequence of rhodopsin (*24*). The value of δ_i is set at 8.4 G, corresponding to the average value of an immobilized, buried residue in a protein undergoing slow rotational diffusion ($\tau_R \geq 30$ ns).

Simulation and Fitting of EPR Spectra. EPR spectra were simulated or fit with the MOMD model of Freed and coworkers using the program NLSL (*14*). A brief description specific to the implementation used in the present work is given below.

In the MOMD model, three coordinate frames are employed to represent the motion of the nitroxide in the protein, as illustrated in Figure 2D. The first is the molecule-fixed magnetic tensor frame (x_M, y_M, z_M). As is customary, z_M lies along the nitroxide p orbital, x_M lies along the NO bond axis, and y_M completes a right-handed coordinate system. The magnetic frame is the principal frame for both the nitroxide hyperfine (**A**) and **g** tensors. The second coordinate frame is the principal frame of the rotational diffusion tensor (x_R, y_R, z_R). In general, the rotational diffusion and magnetic frames are not coincident. The relationship between these frames is specified by the diffusion tilt angles (α_D, β_D, γ_D), defined as the Euler angles required for rotation of the magnetic frame into the diffusion frame. Simulations of the experimental spectra to be discussed below are dependent on β_D (Figure 2D), the tilt angle between z_R and z_M, but only weakly dependent on α_D and γ_D. Anisotropic motions are simulated in the MOMD model by introducing a restoring (ordering) potential (U) that constrains the spatial extent of the motion of z_R. Most spectra of R1(a) and R1(b) on solvent-exposed helical sites of proteins are adequately simulated using the restoring potential $U(\theta) = -{}^1/_2 k_B T C_{20}(3\cos^2\theta - 1)$ to describe the motion of the nitroxide, where C_{20} is a scaling coefficient and θ is the (instantaneous) angle between z_R and the symmetry axis of the potential (*15*). The symmetry axis of the potential defines the z-axis of the third and final coordinate frame, the director frame. For describing the nitroxide side chains on a protein subject to the above ordering potential, the director frame is uniaxial (z_D) and fixed to the protein backbone at the residue of interest. The existence of the restoring potential results in an anisotropic motion and can be characterized by the order parameter $S_{20} = {}^1/_2\langle(3\cos^2\theta - 1)\rangle$, where the brackets indicate averaging over spatial coordinates. The origin of the potential in the X_4/X_5 model is the barrier to rotation about the corresponding bonds of the side chain. For an individual protein molecule, z_D forms an angle ψ with respect to the external magnetic field. To obtain the final spectrum corresponding to an isotropic distribution of protein orientations, the spectra are summed over ψ.

For generating theoretical spectra with the MOMD model, the values for the elements of the **A** and **g** tensors were fixed at $A_{xx} = 6.2$, $A_{yy} = 5.9$, A_{zz}, $= 37$, $g_{xx} = 2.0076$, $g_{yy} = 2.0050$, $g_{zz} = 2.0023$, and the diffusion tilt angles were fixed at $\alpha_D = 0°$, $\beta_D = 36°$, $\gamma_D = 0°$. These parameters were previously found to be optimal for R1(a) on solvent-exposed surfaces of helices (*12*). An isotropic diffusion tensor was used, the principal values of the Lorentzian line width tensor (**W**) were set to zero, and the Gaussian inhomogeneous broadening (gib0) was 1.0 G.

For fitting of experimental spectra, the **A** and **g** tensor elements were fixed at the values given above, and an axially symmetric diffusion tensor was employed, with principal values $R_\parallel$ and $R_\perp$. In this report, spectra are characterized by the geometric mean of the diffusion tensor elements, $\bar{R} = (R_\parallel R_\perp^2)^{1/3}$, and an asymmetry parameter $N = R_\parallel/R_\perp$. The effective mean correlation time, τ, is defined as $\tau = 1/6\bar{R}$. Starting with the Lorentzian line width parameters set to 0 and the Gaussian inhomogeneous broadening at 1 G, $\bar{R}$ was varied to fit the central line width. For the highly mobile essentially isotropic spectra in the basic region of GCN4−58 free in solution (6−20), N and C_{20} were fixed at 1 and 0,

respectively, and $\bar{R}$ and the Gaussian inhomogeneous line width (gib0) were the only parameters varied to obtain a least-squares fit. In the best fit, $\bar{R}$ was close to the initial estimate. The NLSL program does not allow for independent variation of the relative populations of spins in a multicomponent fit, so these fits are highly constrained. At a few sites in the basic region, best fits were obtained by including a Heisenberg exchange rate for the more immobile component. For the less mobile residues in the region of the leucine zipper (25−46), a survey showed that the best fits were obtained with N values ≈ -0.5, and N was fixed at this value in order to constrain the fits and eliminate problems with the correlation between $\bar{R}$ and N.

For R1 in GCN4−58 bound to DNA, the relatively immobilized spectra required finite values of C_{20} for good fits. Following the initial procedure described above, N was again fixed at -0.5 and C_{20} was searched for an approximate fit to the overall line shape. For the final fit, $\bar{R}$, C_{20}, and the Gaussian inhomogeneous line width parameters were varied for a least-squares best fit. A few cases required an additional term in the order potential for a best fit (C_{22}). The parameters $\bar{R}$ and C_{20} may be correlated in the fitting procedure. To estimate the error due to such correlation, $\bar{R}$ was incrementally changed from the best-fit value and C_{20} varied for a new fit. This procedure was continued until the reduced chi-squared for the new fit exceeded that for the best fit by 5%. In this way a range of values for $\bar{R}$ and C_{20} were obtained that provided an estimate for the error in those quantities. This strategy was used for representative cases covering the range of correlation times and ordering potentials encountered, and similar errors were assumed to hold for the other cases. Error estimates obtained by this procedure are larger than those estimated from the chi-squared statistics.

RESULTS

Line Width as a Measure of Mobility. As mentioned above, M_s is a simple spectral parameter based on line width that is used as a measure of side chain mobility. To examine the dependence of M_s on rate and order in single component spectra, a library of simulated spectra was generated using the MOMD model as described in Materials and Methods. To constrain the magnitude of this task, the motional model for the R1 side chain at a noninteracting solvent-exposed site on an α-helix was selected (Figure 2) (*12*, *15*). In general, such helix surface sites do not perturb the protein structure and provide the optimal location for a nitroxide "sensor" of backbone motion.

Figure 4 shows the dependence of M_s on order parameter (S_{20}) and correlation time (τ) and as measured from a subset of the simulated library. The gray regions of the plots highlight the ranges of S_{20} (0−0.5) and τ (1−4 ns) corresponding to values observed for R1 at noninteracting helix surface sites.

The width of the central resonance line, upon which M_s is based, is a function of inhomogeneous proton hyperfine interaction, *g*-factor anisotropy, and motion. In the fast motional regime ($\tau < 0.5$ ns), the *g*-factor anisotropy is averaged, and the inhomogeneous width of ≈1 G is determined by the interaction of the unpaired electron with the protons on the nitroxide ring (*25*, *26*). In the fast motional limit ($0.5 < \tau < 1$ ns), rotational diffusion gives rise to

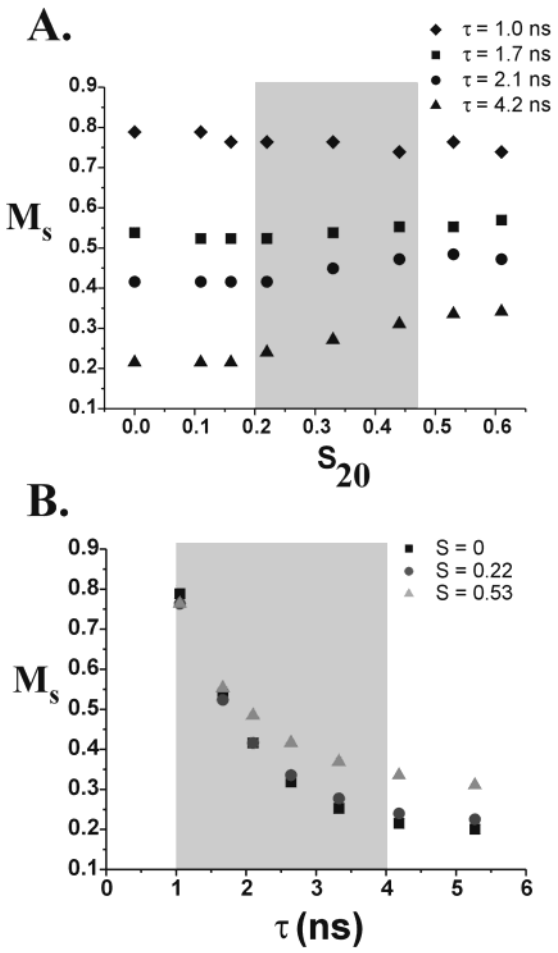

FIGURE 4: Dependence of M_s on S_{20} and τ determined from simulated spectra. (A) Dependence of M_s on the order parameter for the indicated correlation times. (B) Dependence of M_s on the correlation time for the indicated order parameters. The gray boxes highlight the range of values expected for R1(a) on solvent-exposed helical sites.

relaxation effects resulting from the *g*-factor anisotropy, and a Lorentzian contribution to the line width can be computed from Redfield theory (*27*). In the rigid limit ($\tau > 50$ ns), the inhomogeneous line width is determined by the static *g*-factor anisotropy, which corresponds to about 8.8 G at X-band microwave frequencies. In the intermediate motional range ($1 < \tau < 50$ ns), the line widths can be computed from a suitable line shape theory (*28*).

Figure 4A shows that M_s is relatively insensitive to changes in order parameter for values of τ from 1 to 2 ns, a range relevant to R1 on helix surface sites. This is a consequence of the intrinsic internal motion of the nitroxide side chain (i.e., $S_{20} = 0.47$, $\tau = 2$ ns, and $\beta_D = 36°$) that already results in an extensive averaging of the *g*-factor anisotropy at the rates considered. Thus, a reduction in the apparent order parameter due to additional modes of motion will have little further effect. For slower rates ($\tau = 4$ ns) and high order, there is a slight *increase* in M_s with increasing order. In this motional regime, the central line width is dominated by relaxation effects, and the increase in M_s with increasing order parameter could arise from a reduction in relaxation efficiency with increasing anisotropy of motion, causing the spectra for larger S_{20} to have a narrower center line. M_s is extremely sensitive to τ for all values of S_{20} investigated in the range of 1−4 ns (Figure 4B). The conclusion from these

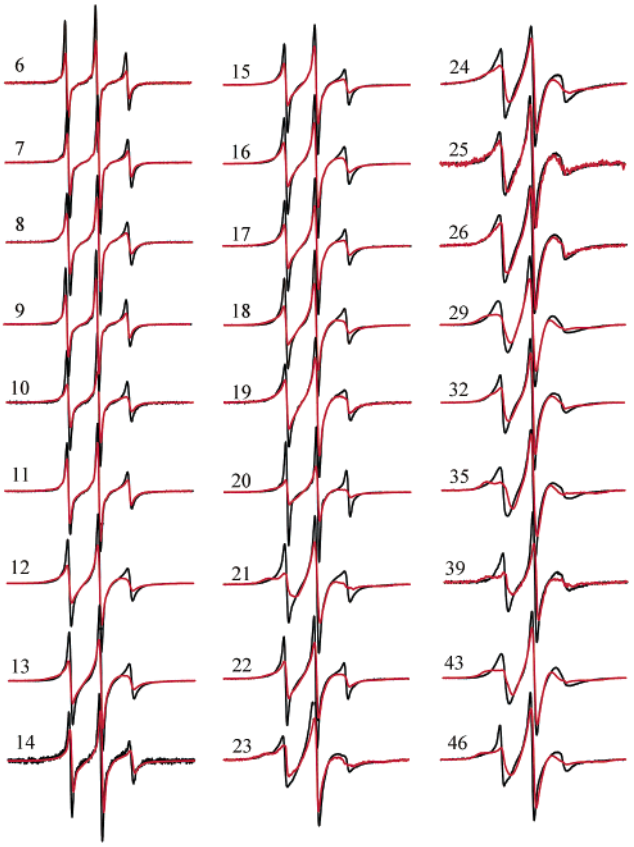

FIGURE 5: Experimental EPR spectra of the GCN4−58 dimer free in solution. The spectra of R1(a) (black) and R1(b) (red) at the indicated sites are shown superimposed. The spectra of 23R1(a) and 23R1(b) correspond to magnetically dilute samples.

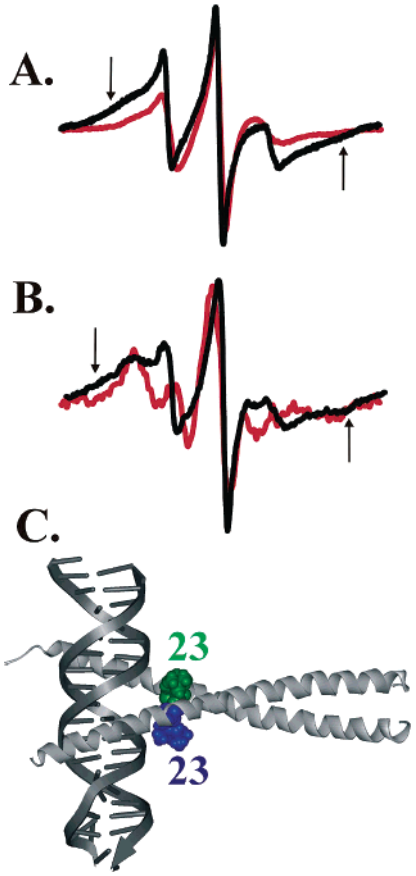

FIGURE 6: Spin−spin interactions in GCN4−58. (A) EPR spectra of the 23R1(a) homodimer (black) and 23R1(a) diluted with unlabeled wild type (red), both free in solution. The spectra are normalized to the central line to emphasize the difference in line shape. (B) EPR spectra of 23R1(a) (black) and 23R1(a) diluted with unlabeled wild type (red) bound to 2AP-1. The arrows in (A) and (B) indicate regions of intensity that arise from spin−spin interactions. (C) A ribbon model of GCN4−58 bound to DNA based on the crystal structure (*21*) showing 23R1(a) residues as space-filling models.

results is that the commonly used measures for relative mobility (δ^{-1} and the derived M_s) are primarily measures of relative *rates* when applied to R1(a) at helix surface sites. The results of Figure 4 apply to single-component spectra. For spectra with two components corresponding to similar numbers of spins with significantly different mobilities, M_s is dominated by the most mobile component.

Motion of R1(a) and R1(b) in GCN4−58. In previous work, it was shown that the internal motion of the R1(b) side chain on an α-helix is reduced relative to that in R1(a) due to interactions of the 4-methyl group, presumably a steric clash with the S_γ of the disulfide bond (*12*). That being the case, dynamic contributions from the backbone would contribute in larger proportion to the overall motion of the nitroxide in R1(b) relative to R1(a). In the present experiments, both R1(a) and R1(b) were used to probe backbone motions in GCN4−58 to evaluate this possibility.

Figure 5 shows the EPR spectra of R1(a) (black) and R1(b) (red) for a continuous scan through the basic (DNA-binding) region of GCN4−58 (residues 6 through 26) and for selected solvent-exposed sites in the leucine zipper region (29, 32, 35, 39, 43, and 46). The locations of the sites in the molecule are shown in Figure 3. The spectra for R1(a) and R1(b) at each site are normalized to the same number of spins, and the relative amplitude is a sensitive indication of differences in rates of motion. The EPR spectra have very narrow line widths, particularly in the basic region, indicating very high mobility of the R1 side chain. As will be shown below, this motion is dominated by internal motions within the protein, with smaller contributions from the overall tumbling of the 13 kDa GCN4−58 dimer.

EPR spectra of GCN4−58 27R1(a) and 27R1(b) were also recorded but not included in Figure 5 because the spectra reflected unusually high mobility, suggesting lack of dimer formation, and the mutants did not bind DNA substrate. This is not surprising, because methionine 27 is at the dimer interface at the beginning of the leucine zipper region, and the presence of the larger spin label could destabilize the protein. In addition, this residue is thought to play a specific role in the DNA-binding reaction (*29*). Within the leucine zipper region, only sites on the outer surface of the helices were selected, to avoid disruption of the coiled coil by introducing a bulky side chain at the packing surface. Under any circumstance, the surface sites are the important ones for sensing backbone motion, the subject of the present study.

The EPR spectrum of R1(a) at site 23 in the homodimer showed clear evidence of spin−spin interaction in the broad "wings" of the spectra (*30*, *31*) (arrows, Figure 6A), with a weaker but noticeable interaction in 24R1(a) (Figure 5). This was tested in 23R1(a) by the addition of a 5:1 excess of unlabeled wild-type GCN4−58. If subunit exchange in

GCN4−58 takes place, the equilibrium mixture would have only 2.8% of dimers with two spins, and the interaction should greatly decrease. This in fact is the result, as seen by the decrease in the spectral amplitude in the wings (Figure 6A, red trace), simultaneously confirming the presence of strong spin−spin interaction in the homodimer as well as subunit exchange.

An estimate of the interspin distance obtained from the spectral broadening in the 23R1(a) homodimer (≈6−7 G) gives a range of 10−15 Å (*30*). Modeling of the R1(a) side chain in a preferred conformation (X_1, $X_2 = g^+, g^+$) (*16*) in the structural model of GCN4−58 derived from the crystal structure of GCN4−58 bound to DNA (shown in Figure 6C) indicates that the nitroxide side chains point away from each other on opposite sides of the dimer, with an inter-nitroxide distance of ≈15 Å, consistent with the distance estimated from spin−spin interaction. Other residues of the basic region forming topologically homologous pairs to 23, for which spin−spin interaction might occur, are 20 and 27. For 20R1(a), there is a slight reduction in the spectral breadth when the sample is diluted with unlabeled wild-type protein (data not shown), and spectral fits of 20R1(a) required the inclusion of weak Heisenberg exchange, indicative of weak interaction between the nitroxide spins (see below). A weaker interaction compared to 23R1(a) is indeed expected on the basis of the crystal structure, because the putative helical segments diverge spatially from residue 23 to residue 20 (see Figure 3). As mentioned above, 27R1(a) did not form dimers and could not be tested for spin−spin interaction.

Plots of the scaled mobility of the spectra versus sequence for R1(a) and R1(b) are shown in Figure 7A, where it is apparent that the basic DNA-binding sequence (6−28) and the leucine zipper region (29−46) are clearly delineated by R1(a) and R1(b) on the basis of M_s. In the DNA-binding region, an overall gradient of mobility is observed for both R1(a) and R1(b) side chains, in which the highest mobility is at the N-terminus.

Superimposed on the gradient for R1(a) is a weak oscillation in M_s in the region between residues 8 through 20 that has a period of 3−4 residues, suggesting an average α-helical conformation. The residues at the local maxima in M_s for R1(a) are identified with open symbols (6, 9/10, 14, 17, 20, and 23) in Figure 7A. Except for 20, these residues correspond to the residues on the outer surface of the helix identified in the crystal structure (Figure 3). A similar oscillatory pattern of larger amplitude is observed in M_s for R1(b).

Several lines of evidence suggest that the motions of R1(a) along the basic region as reflected by M_s are dominated by internal motions rather than the rotational diffusion of the protein as a whole (the "uniform mode"). The first is the existence of the mobility gradient itself, which would not be observed if the uniform mode dominated. Further evidence is provided by the response of the side chain motion to selective perturbation of the internal and uniform modes. Selective perturbation of the internal modes of R1(a) by addition of the 4-CH_3 group to the nitroxide ring, which was previously shown to restrict internal rotations about X_4/X_5, results in a reduction of mobility at all sites as measured by M_s, and the gradient is preserved (Figure 7A). Because the addition of a single CH_3 group would not affect the uniform modes, this result indicates the importance of internal modes

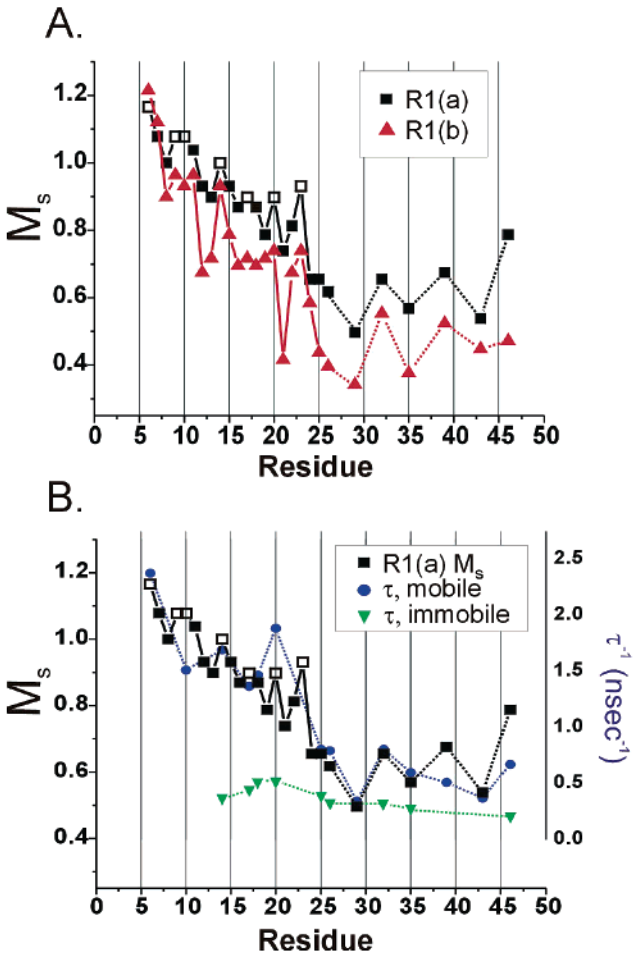

FIGURE 7: Backbone dynamics for GCN4−58 free in solution. (A) M_s for R1(a) (black squares) and R1(b) (red triangles) as a function of sequence. Open symbols indicate maxima in scaled mobility for R1(a). (B) Values for τ^{-1} for the mobile (blue circles) and immobile (green triangles) populations of R1(a) are plotted versus residue. The τ values were obtained from fits to the spectra. Due to the highly constrained fitting procedure, no error is associated with the τ values. M_s values of R1(a) are shown for comparison. Dashed lines indicate nonsequential connections between data points.

within the side chain in determining the nitroxide motion.

Selective perturbation of the uniform mode can be achieved by increasing the viscosity of the medium. In studies on globular proteins of similar molecular mass (T4L), the contribution from rotational diffusion was reduced by the addition of sucrose to increase the viscosity. Due to the possible effects of osmotic stress on this poorly packed protein, this strategy was not employed, but Ficoll 70 was used instead. At 30% w/v, Ficoll 70 has low osmolarity but produces an equivalent viscosity to 30% w/v sucrose with regard to rotational diffusion of T4L (4.8 cP) (Guo and Hubbell, unpublished results). Ficoll 70 at this concentration has no effect on the EPR spectra of the sites sampled in the basic region of GCN4−58 (10, 17, 18, 25; data not shown). If the uniform mode contributed to the EPR line shape, a significant reduction in correlation time for the nitroxide would be expected. Together, the above data suggest that the dynamic properties of the nitroxide side chains deduced from M_s in the basic region are those arising primarily from internal motions.

The dynamics of the R1 side chains can be further analyzed by least-squares fitting of the spectra to the MOMD

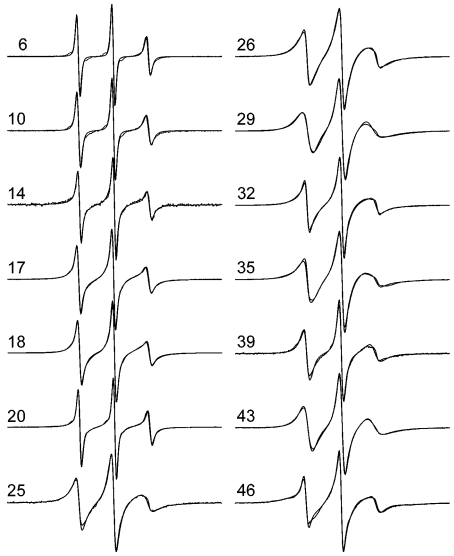

FIGURE 8: Experimental spectra and theoretical fits of R1(a) at solvent-exposed helical sites in GCN4−58. The experimental spectra of R1(a) for GCN4−58 free in solution are shown in black, and the MOMD least-squares best fits are overlaid in gray lines.

model of Freed and co-workers (*14*) and compared with M_s. Fits to selected spectra spanning the basic region and corresponding to local maxima in M_s (6, 10, 14, 17, 18, 20, 25, and 26) are shown as gray dashed traces in Figure 8. In each case, the best fits are obtained with an order parameter $S_{20} = 0$ and isotropic diffusion rates. The values for the best-fit parameters for these and other sites discussed below are provided in tabular form in Supporting Information. For R1(a) at sites 14, 17, 18, 20, 25, and 26, two populations with different correlation times were required. For sites 17, 18, 20, and 26, fits to the more immobile component required a broadening that could be accounted for by weak Heisenberg exchange between spins. Alternatively, the broadening could be accounted for by relaxation effects arising from motional modulation of a dipolar interaction. Either way, the result implies that the spins are in proximity in the more immobilized state.

In the presence of multiple components, M_s is determined by that with the largest diffusion rate (narrowest line), and as will be discussed below, this is the relevant component for monitoring backbone motion. For this component the diffusion rates determined from fitting are in the range $1 \times 10^8\ s^{-1} \leq D \leq 4 \times 10^8\ s^{-1}$, about an order of magnitude faster than the uniform modes for diffusion of GCN4−58 estimated from NMR ($D_{\|} = 2.13 \times 10^7\ s^{-1}$; $D_{\perp} = 1.11 \times 10^7\ s^{-1}$) (*17*). Again, this supports the notion that internal motions, not overall rotational diffusion, are dominant in determining the EPR spectral line shapes, at least for the most mobile component.

In the leucine zipper region, sites for introduction of R1(a) and R1(b) were selected to lie on the solvent-exposed surface of the coiled-coil structure to monitor backbone motions (29, 32, 35, 39, 43, and 46; see Figure 3). As measured by M_s, the motions of R1(a) and R1(b) in this region are clearly damped relative to those in the basic region. The spectra of R1(a) at these sites can be reasonably well fit to the MOMD model, as shown by gray dashed traces in Figure 8. For all but 29R1(a) and 43R1(a), $S_{20} = 0$ and two populations with different diffusion rates are required for the best fit. The diffusion rates of the most mobile component determined from the fits are in the range $6.3 \times 10^7\ s^{-1} \leq D \leq 1.7 \times 10^8\ s^{-1}$. These rates are sufficiently slow that the uniform modes of the protein could affect the EPR line shapes. To examine this possibility, the viscosity of the solution for representative sites 29R1 and 43R1 was increased to 4.8 cP with 30% w/v Ficoll. The resulting EPR spectra could be well fit with the same parameters used for buffer, but with an increase in correlation time of ≈15% in each case. This small effect suggests that the internal motions in the protein again dominate the EPR spectra and that contributions of the uniform mode are small, at least for spin populations with diffusion rates in the above-mentioned range. At sites where the spectra of R1(a) have multiple components, both in the basic and in the zipper regions, the components corresponding to the most immobilized state have diffusion rates in the range $3.1 \times 10^7\ s^{-1} \leq D \leq 7.4 \times 10^7\ s^{-1}$, where protein rotation will have a significant effect on the spectral line shape. For these sites, the SRLS model of Freed (*32*) would be required for fits to the experimental data in order to extract the internal modes, and these cases are not treated here.

For monitoring backbone dynamics, the most useful site for placement of an R1 side chain is at a solvent-exposed surface where the side chain makes no tertiary contacts and perturbation to the structure is minimal. These sites are identified in Figure 3 and in the basic region corresponding to the local maxima in the plot of Figure 7A. To compare the dynamics of the R1(a) side chain at such sites as determined by M_s and fitting, the diffusion rates for the most mobile component, determined by fitting and expressed as τ^{-1}, where τ is the effective nitroxide correlation time, are plotted in Figure 7B. As is evident, both M_s and τ^{-1} reflect the same motion. The diffusion rates, τ^{-1}, for the immobile components are relatively constant throughout the sequence and are shown in Figure 7B for comparison. A possible origin of the immobilized sites and the regular variation in mobility of sites along the zipper will be discussed below.

The above results indicate that the basic region is, on the average, helical, but flexible on the nanosecond time scale, with sufficient amplitude of motion to reduce S_{20} of the nitroxide from an expected value of 0.47 [that for the T4L 72R1(a) reference corresponding to internal side chain motions] to ≈ 0. The leucine zipper region has more ordered structure, consistent with earlier NMR and CD studies (*17*, *22*).

Dynamics of the R1 Side Chains in GCN4−58 Bound to DNA. Figure 9 shows the EPR spectra of residues in GCN4−58 labeled with R1(a) (black) and R1(b) (red) bound to 2AP-1 DNA. As is evident in a comparison of Figures 5 and 9, dramatic spectral changes take place for R1 residues throughout the basic region from residues 6−28, and to a lesser extent along the leucine zipper region, upon DNA binding. GCN4−58 derivatives 11R1(a and b), 12R1(a and b), 14R1(a and b), 16R1(a and b), and 18R1(b) did not bind to the DNA substrate as evaluated by SDS gel-shift assay, and the EPR spectra did not change upon addition of the substrate. Thus, the spectra are not included in Figure 8. These sites occur at the DNA-binding interface and are shown in Figure 10. The labeled sites that bound DNA are also indicated by their sequence number in Figure 10.

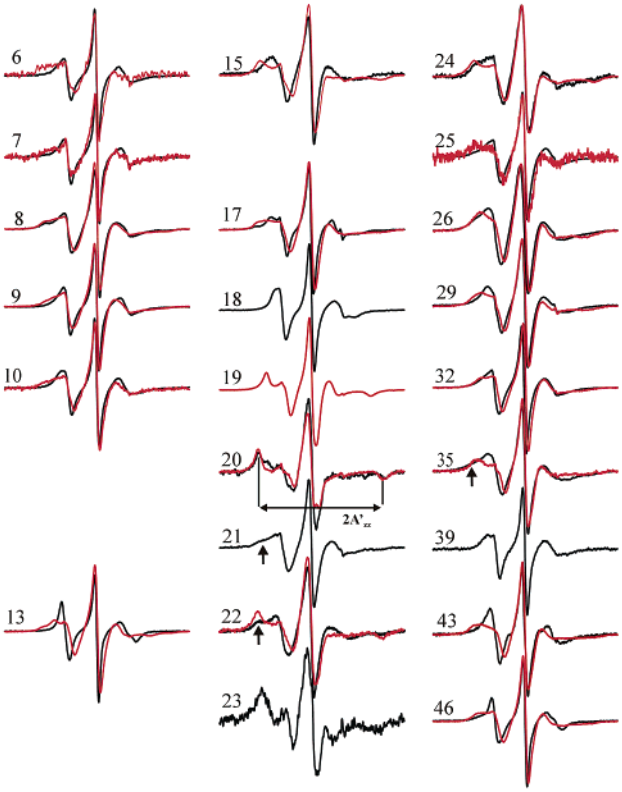

FIGURE 9: EPR spectra of R1(a) in GCN4−58 bound to 2AP-1. The experimental EPR spectra of R1(a) (black) and R1(b) (red) at sites in the DNA-binding region (6−26) and at solvent-exposed helical sites in the leucine zipper of GCN4−58 are shown. Missing residues either did not bind DNA or precipitated upon the addition of DNA. The hyperfine splitting $2A'_{zz}$ is indicated on the spectrum of residue 20. Arrows indicate immobilized spectral components discussed in the text. The spectrum of 23R1(a) is of the magnetically diluted sample.

The pattern of mobility changes upon DNA binding is more clearly revealed in Figure 11, which shows plots of M_s versus sequence for R1(a) and R1(b) on GCN4−58 bound to 2AP-1 together with the corresponding plots of the free form for comparison. Remarkably, the overall gradient of mobility along the basic region is retained in the DNA-bound form. A continuous sequence of labeled sites is not available for the DNA-bound form, but for R1(a) from 20 to 26 a regular helical pattern is observed that is in excellent agreement with the crystal structure This pattern differs in phase from that in the free protein in the 20−25 sequence, indicating a difference in structure in this region. Without DNA bound, the highly positively charged region may have significant repulsion between the monomers (which are in close proximity between residues 20 and 25) to distort the helical structure.

In the leucine zipper region, relatively small changes in mobility are seen between the unbound and bound forms. These results show that the basic region becomes more ordered upon binding to DNA, while the structure and dynamics of the leucine zipper region are comparatively unchanged. The fact that DNA binding reduces the rate of the uniform modes of GCN4−58 but does not change the dynamics of the leucine zipper may be taken as support for the earlier conclusion that uniform modes contribute little to the dynamics of side chains in the unbound state.

FIGURE 10: A model of GCN4−58 bound to DNA substrate 2AP-1. The spin-labeled sites are represented with spheres, and the solvent-exposed helical sites are labeled and colored green on the upper protein molecule. On the bottom, CPK models of residues 11 (green), 12 (yellow), 14 (cyan), and 16 (orange) are shown. The model was generated on the basis of the crystal structure of GCN4 bound to AP-1 (PDB id: 1YSA).

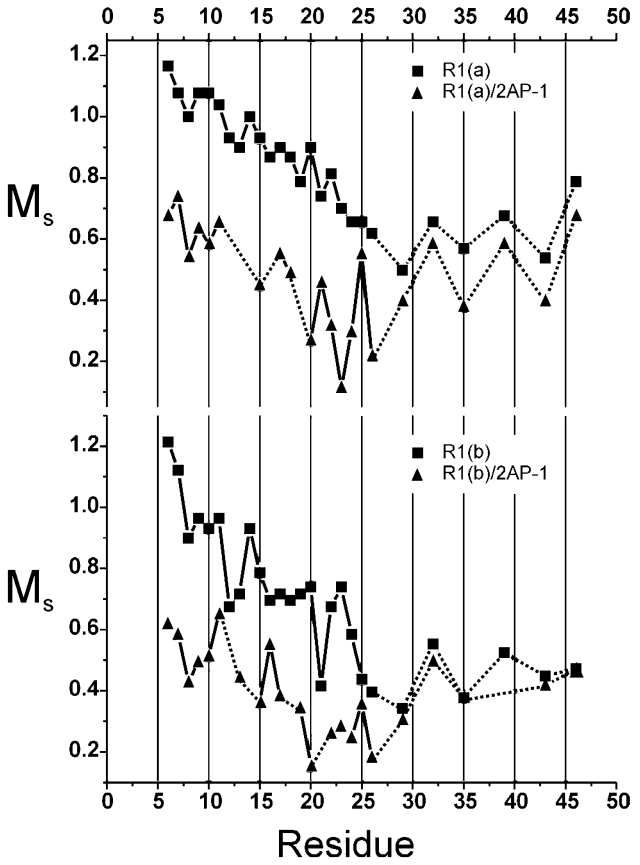

FIGURE 11: Comparison of M_s between free and DNA-bound forms of GCN4−58. M_s is plotted versus residue for R1(a) (top) and R1(b) (bottom) for the DNA-bound (triangles) and free (squares) forms of the protein. Dashed lines indicate nonsequential connections between data points.

The 2AP-1 construct contains two GCN4−58 binding sites and was chosen because the molecular mass of the complex

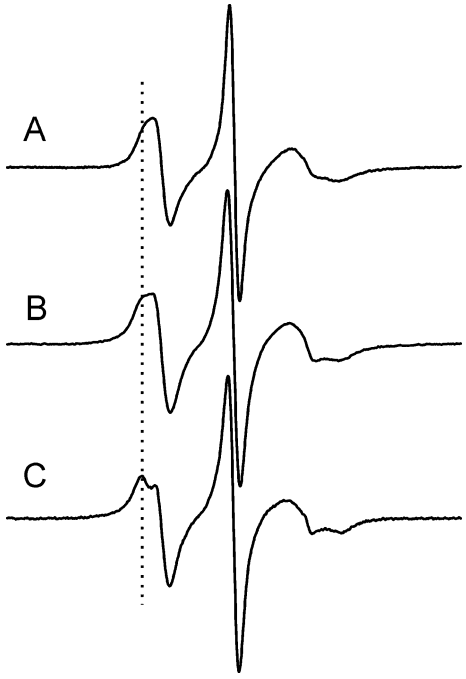

FIGURE 12: Effect of changing the uniform modes on the motion of 18R1(a) in GCN4−58 bound to DNA. EPR spectra are shown for 18R1(a) in GCN4−58 bound to AP-1 in buffer (A), bound to 2AP-1 (B), and bound to AP-1 immobilized on streptavidin−agarose beads (C). The vertical dashed line is drawn as a reference to guide the eye for comparison.

is high (≈50 kDa); hence, the correlation time of the complex is expected to be slow on the EPR time scale, and only internal motions of the side chain and backbone fluctuations should contribute to the EPR spectra. A lower limit to the correlation time of the complex can be determined using the EPR spectrum of 20R1(b). This side chain is buried in the interior of the complex (in agreement with the crystal structure) and, therefore, immobilized relative to the protein. Using a Brownian diffusion model and the measured $2A'_{zz}$ (labeled in Figure 9), the correlation time of the nitroxide of 20R1(b) is estimated to be 16.8 ns (*28*). This value is similar to that calculated from the Stokes−Einstein equation for a sphere of equivalent mass (16.5 ns).

To further demonstrate that the contribution of the rotational diffusion of the protein/DNA complex does not significantly contribute to the EPR line shape, the uniform modes were modulated. Figure 12 shows three spectra of GCN4−58 18R1(a): (A) bound to AP-1 (a smaller DNA construct with one binding site); (B) bound to 2AP-1, and (C) bound to AP-1 immobilized by attachment to streptavidin beads at the 5′-end of one strand. Compared to GCN4−58 18R1(a) in solution, all of the DNA-bound spectra have reduced mobility. Uniform rotational diffusion modes of the AP-1/protein complex should be absent when bound to streptavidin beads, and the EPR spectrum should reflect exclusively internal motions within the protein. In this case, the spectrum of 18R1(a) has a line shape characteristic of anisotropic motion (Figure 2D). The small splitting of the $A_{||}$ and $A_{\perp}$ hyperfine components of 18R1(a) makes this line shape very sensitive to averaging by additional motions. Compared to this as a reference, the line shape of GCN4−58 18R1(a) in the 2AP-1 complex is very similar, but with slightly less resolved hyperfine extrema, presumably due to a small effect of the uniform modes of the 2AP-1 complex.

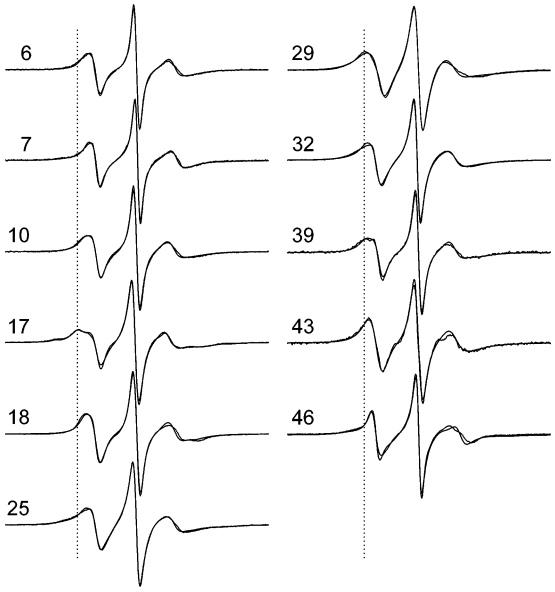

FIGURE 13: Experimental spectra and theoretical fits for R1(a) at the indicated sites in GCN4−58 bound to 2AP-1. Experimental spectra are shown in black, and the least-squares best fits to the MOMD model are shown in gray lines. The vertical dashed line is drawn as a reference to guide the eye for comparison.

The smaller AP-1/protein complex shows an additional incremental motional effect, but it is still rather small. Collectively, the results presented in the preceding paragraphs indicate that the motions of R1 in the GCN4−58/2AP-1 complex faithfully report internal modes of motions, largely uninfluenced by overall tumbling.

To monitor backbone dynamics, the outer helix surface sites bearing a spin label, facing away from the DNA-binding site, were selected for further analysis. Of the sites studied, R1(a) at residues 6, 7, 10, 17, 18, 21, 22, 25, 29, 32, 35, 39, 43, and 46 does not perturb binding. The line shapes of 10R1(a), 17R1(a), 18R1(a), and 39R1(a) bound to 2AP-1 show resolved or partially resolved parallel and perpendicular hyperfine extrema, characteristic of the weakly ordered anisotropic motion observed at many solvent-exposed helical sites (*12*, *13*, *15*). The spectra of the 21R1(a) and 22R1(a) side chains are complex, with a dominant immobilized component suggesting interactions with the local environment (arrows in Figure 9). Due to the extent of the interaction, such sites may not be suitable for monitoring backbone dynamics in isolation and are not further considered. For 35R1(a), the tails in the spectrum (arrows in Figure 9) suggest a possible spin−spin interaction, and this residue is also excluded.

The best fits to the MOMD model for all outer helix surface sites except 21R1(a), 22R1(a), and 35R1(a) are shown by the gray dashed traces in Figure 13. Figure 14 provides a graphical representation of the motional rates and orders, derived from fitting, compared with the corresponding M_s values. Error bars for the fit parameters are shown for a few of the values in Figure 14, and similar errors are expected for the other fit parameters in the figure. Given the errors, all trends and gradients discussed are statistically significant.

The rates, represented as τ^{-1}, are closely correlated with M_s. Where two dynamic components are required for the fits, the most mobile is used to construct the plot, since it is this component that determines M_s and most directly reflects

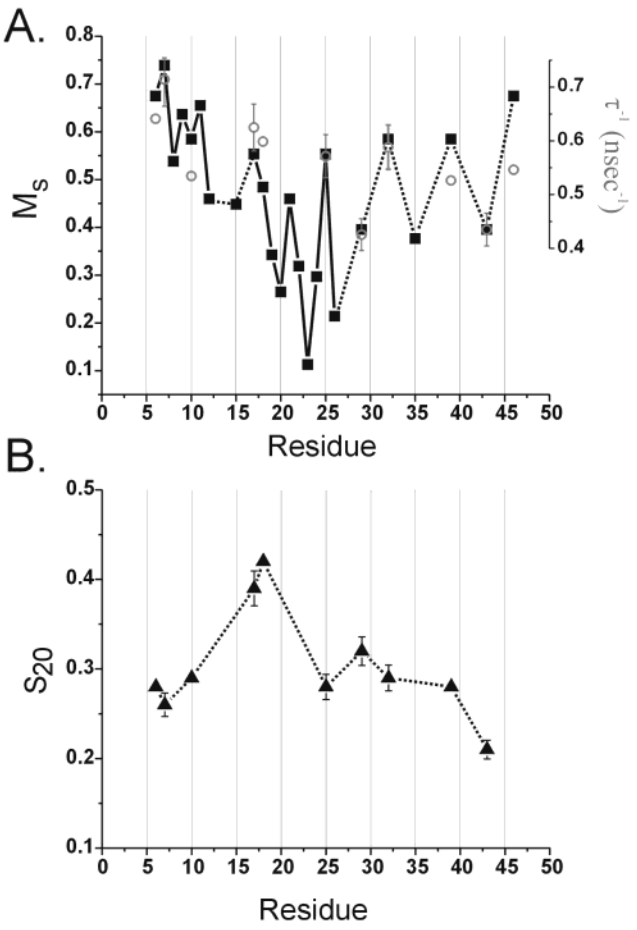

FIGURE 14: Comparison of scaled mobility, τ^{-1}, and S_{20} for GCN4−58 bound to 2AP-1. The experimentally determined scaled mobility (black squares, A) and the τ^{-1} (gray open circles, A) and S_{20} (black triangles, B) values derived from the fits in Figure 13 are plotted versus sequence. Error bars for τ^{-1} and S_{20} were estimated as described in Materials and Methods for representative cases. Similar errors are expected for the other values.

backbone motions (see Discussion). The order parameter S_{20} shows a gradient increasing from residue 6 to a maximum at the DNA-binding site (residues 17 and 18), inversely correlated to that of the M_s gradient. At the binding site, the order parameters are 0.42 and 0.40, close to that for the internal motion of the side chain alone (≈0.47), and the backbone has adopted a highly ordered conformation in this region. The spectrum of 18R1(a) is unusual in that the best fits require higher order terms than C_{20} in the ordering potential (C_{22}), and the *z*-axis diffusion rates of the nitroxide are higher relative to the *x* and *y* rates compared to R1(a) at other sites. The origin of this difference is not obvious from the structure of the GCN4−58/DNA complex, but the potential may be influenced by the proximal highly charged DNA backbone. In the leucine zipper region, the order parameters are relatively constant and drop off at residue 46.

Spin−Spin Interaction. In the spin-labeled homodimer bound to 2AP-1, 23R1(a) has extremely broad spectra with overall width extending beyond 100 G, indicating strong spin−spin interaction between the nitroxides in the two chains (Figure 6B). As described above for the unbound protein, magnetic interaction was confirmed for 23R1(a) by the disappearance of the interaction upon a 5× dilution of the sample with the unlabeled wild-type protein (Figure 6B). The presence of a strong interaction is consistent with the crystal structure of the complex shown in Figure 6C, which places residues at position 23 in close apposition.

DISCUSSION

The purpose of the present work has been to explore the potential of SDSL for monitoring backbone dynamics using a simple model system, GCN4−58, that has been characterized by NMR relaxation methods. The strategy for detecting helical backbone motions is based on knowledge of the internal dynamic modes of the R1 family of side chains at solvent-exposed helix sites and the assumption that this mode is similar at structurally homologous sites. The internal mode of the R1 side chain at such sites, as it is currently understood, is illustrated in Figure 2. The motion is distinguished by rapid (1−2 ns) internal motions about the bonds of the side chain that give rise to partial averaging of the hyperfine **A** and **g** tensor elements. The resulting EPR spectrum has a characteristic anisotropic line shape that can be characterized by an order parameter and a correlation time. An important point is that the internal motions of the side chain only *partially* average the **A** and **g** values. The residual, unaveraged, magnetic parameters can then be further averaged by segmental backbone modes of the protein, providing a means for their detection. Although the intrinsic order parameter and correlation time that characterize the side chain internal modes are not known with certainty, values of these parameters for R1(a) at site 72 in T4L ($S_{20} = 0.47$; $\tau = 2$ ns) are tentatively taken as the first approximation to represent the internal modes, as discussed previously (*12*). Thus, decreases in the order parameter and/or increases in the rate are attributed to segmental backbone motions.

Scaled Mobility as a Sensor of Backbone Dynamics. The spectra of the R1 side chains on GCN4−58 can be fit reasonably well with the MOMD model to provide effective correlation times and order parameters for detecting contributions from backbone motions. However, for analyzing large data sets, it is convenient to have simple parameters determined directly from the spectra that reflect the nitroxide motion. As shown in Figure 4, M_s, based on the central line width, provides a measure of the rate of motion for the line shapes encountered for R1 on helical sites. In the multicomponent spectra that often arise, M_s is largely determined by the most mobile component, and in general, this is the component of interest for monitoring backbone motions. The more immobile components have correlation times longer than that for the intrinsic internal motion of the R1 side chain and likely arise from interactions of the nitroxide with the protein environment. Thus, they do not directly reflect modulation of the internal modes by backbone motion, and it is an advantage that such modes do not dominate M_s. In the paragraphs below, the spectral data sets from GCN4−58 will be discussed from the point of view of theoretical fits and M_s.

Structure of GCN4−5 in Solution. The structures of the GCN4−58 dimer and the leucine zipper domain in solution have been investigated by CD (*22*) and NMR (*17*, *33*, *34*). The $^{13}C^{\alpha}$ and ^{13}CO secondary chemical shifts show conclusively that the coiled-coil leucine zipper region is strictly α-helical. On the other hand, α-helical sequential NOEs were not observed in the basic DNA-binding region preceding

residue 25, eliminating the possibility that stable helices exist. Nevertheless, intermediate positive $^{13}C^{\alpha}$ and ^{13}CO secondary chemical shifts in the DNA-binding region suggest that α-helical conformations are preferentially populated, leading to the conclusion that the basic region is an ensemble of nascent helices and interconversion between the helical states occurs on time scales faster than microseconds.

In the spin-labeled protein, the weak periodic modulation of M_s with a period of 3−4 residues along the continuous series of sites in the basic region likely reflects the presence of a helical structure (Figure 7), although the depth of modulation is far less than observed for helices in well-packed proteins (*10*). In addition, the strong spin−spin interaction between residues at position 23, and the weaker interaction between those at position 24, also supports the helical configuration in this region. These results are not at odds with the view that GCN4−58 in solution is a collection of rapidly exchanging conformations with a helical preference. If conformations in an equilibrium mixture have lifetimes of $\approx 10^{-7}$ s or longer, EPR spectra characteristic of each state will be observed in proportion to the abundance of that state. The existence of two dynamic populations of the R1(a) side chain at many sites in the basic region may in fact arise from GCN4−58 conformers that are exchanging on this time scale. If so, one conformer is characterized by relatively low and constant R1(a) mobility along the basic region (Figure 7B, green trace) and weak Heisenberg exchange between some of the R1(a) residues in the homodimer. These features suggest a relatively condensed structure with intramolecular interactions between the monomers along the basic region. The other conformer is characterized by the most mobile state of the side chain with a mobility gradient along the basic region. Alternatively, the two dynamic populations of R1(a) could correspond to different rotamers of the R1(a) side chain, one of which has local intramolecular interactions that give rise to the more immobilized population. Irrespective of the origin of the immobilized population, it is the most mobile population measured by M_s that is analyzed in the current study and discussed below.

Backbone Dynamics of GCN4−58: Comparison between NMR and SDSL Data. Backbone dynamics of GCN4−58 have been investigated by reduced spectral density mapping of ^{15}N relaxation data on GCN4−58 in solution (*17*). The data revealed a nearly linear decrease in mobility, measured by $J(0.87\omega_H)$, from the N-terminus to about residue 29, the first residue of the leucine zipper. Throughout the leucine zipper region (29−52) $J(0.87\omega_H)$ was high and essentially constant. The spectral density $J(0.87\omega_H)$ depends strongly on $1 - S^2_{NH}$, where S_{NH} is the order parameter for motion of the backbone NH bond vector. Thus, the ordering of the backbone motion increases regularly from the N-terminus through the basic region. In the leucine zipper region, S^2_{NH} was found to be ≈0.91, typical of ordered helices in other proteins. At a temperature of 290 K, near the temperature where the EPR spectra were recorded in the present experiments, the spectral density $J(\omega_N)$ varied strongly with sequence position along the basic region but was again constant in the leucine zipper. This result suggests a sequence-dependent variation of the rates as well as the order of motion through the basic region, but not in the leucine zipper (*17*).

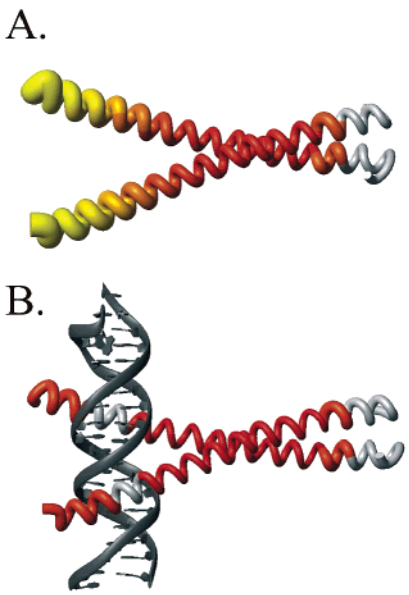

FIGURE 15: Scaled mobility mapped onto the structure of GCN4−58. The width of the backbone tube is directly proportional to M_s in the unbound (A) and bound (B) forms of GCN4−58. The color gradient is from yellow (most mobile) to red (least mobile). The M_s value of each solvent-exposed helical site was used for the respective helical turn in the DNA-binding region. An average M_s was calculated for the leucine zipper (residues 27−41) using sites 29, 32, 35, and 39. The M_s values for sites 43 and 46 were used for their respective helical turns. For the N-terminal sites that were not investigated, but are in the crystal structure, the M_s value for site 7 was used. One solvent-exposed helical site (residue 14) did not bind DNA, and therefore, the backbone of the represented helical turn is colored gray. In addition, data were not collected for C-terminal residues beyond residue 46; this region is also colored gray.

The variations of M_s and τ^{-1} along the GCN4−58 sequence also identify a gradient in mobility (Figure 7). The running average of M_s taken over a window of 3−4 residues (one turn of the putative helix) shows an essentially linear decrease through the basic region, to about residue 29. Residues at the outer face of the helix, those at the local maxima in M_s, are most suitable for single-site monitoring of backbone dynamics, and M_s for these sites also decreases approximately linearly through the basic region. Figure 15 shows a graphical representation of these latter data. Values of τ^{-1} for R1(a) at these sites, determined from fitting (Figure 7B), are in good agreement with the M_s values, supporting the use of M_s as a simple parameter to monitor relative nitroxide rates.

Within the leucine zipper region, R1 residues were only substituted at sites on the outer helical surfaces. For these sites M_s, and to some extent τ^{-1}, shows a regular alternation between high and low values, with 32, 39, and 46 having high and 29, 35, and 43 having low values. The pairwise average values of these residues is relatively constant through the leucine zipper. Residues 32, 39, and 46 are separated by the heptad repeat of the coiled coil, and the C^{α} of these residues lay along a line furthest from the contact surface with the other helix of the coiled coil, while the C^{α} of 29, 35, and 43 are in closer proximity to the contact surface. One model for the alternation in M_s is that the most mobile component of the spin populations at these sites is detecting the difference in backbone dynamics due to differences in contact interactions. The unusually high M_s and τ^{-1} for

46R1(a) reflects the presence of a highly mobile population (≈32%) that could arise from a local unfolding due to the proximity of the C-terminus, which is known to be unfolded (residues 54−58) (*17*).

At all residues in the basic and leucine zipper regions, the spectra of R1(a) can be reasonably well fit without an ordering potential, i.e., with isotropic motion. Thus, it is not possible to examine the sequence dependence of the order parameter using R1(a). This situation is due to the fact that rapid internal motions within the side chain lead to extensive averaging of the **A** and **g** tensors, and relatively little additional mobility from backbone motions is needed to effectively average the residual anisotropy. One solution to this problem is to reduce the amplitude of the intrinsic internal side chain motions by addition of a substituent on the 4-position of the nitroxide ring (*12*), thus extending the dynamic range for detection. For this reason, R1(b) was also investigated in the present study. The 4-CH_3 group of R1(b) increases the intrinsic order parameter for the internal motion from $S_{20} = 0.47$ for R1(a) to $S_{20} = 0.81$. However, for residues 6−20 in the basic region of free GCN4−58, the residual anisotropy is still effectively averaged, and the line shapes remain essentially isotropic. Approximate simulations based on the effective Hamiltonian model for R1 motion (*35*) suggest that nanosecond backbone motions with an order parameter of $S_{20} \leq 0.2$ are required to reduce the internal order parameter from 0.81 to effectively 0. The NMR-based order parameters for the NH bond motion in this same region are $S_{20} \leq 0.6$, but it must be recalled that motions involving rotations about the NH bond axis (axial helix rocking) are not detected in the NMR experiment, while such motions are effective in producing spectral averaging of R1 (*13*). Thus, estimated order parameters for backbone motions derived from motions of R1(a) will in general be less than those determined from $^{15}N-H$ relaxation experiments.

Within the leucine zipper region, addition of the 4-CH_3 group has the desired effect, and spectral line shapes characteristic of anisotropic motion are observed. As always, analysis of such spectra in terms of backbone dynamics requires that the nitroxide not make interactions with the environment. This limits the use of the 4-substituted derivatives, because the substituent itself provides additional opportunities for such interaction, as is evident in many of the spectra in Figures 5 and 9. Future development of spin labels with highly hindered internal modes without additional interactions should greatly improve measurement of dynamic disorder due to backbone motions. However, the line shapes of 29R1(b) and 35R1(b) suggest simple noninteracting states. Fitting of the 29R1(b) and 35R1(b) spectra provides effective order parameters of 0.28 and 0.47, respectively (Figure 16). The additional motion that reduces the order parameter for the intrinsic internal motion from 0.81 to the above values is a quantitative measure of the amplitude of backbone motions, along with a minor contribution from the uniform rotational modes of the protein.

Structure and Dynamics of GCN4−58 Bound to DNA. Not surprisingly, substitution of the native residue by the spin label at several sites within the binding domain perturbs the interaction, and it was not possible to obtain continuous sequences for secondary structure determination. However, for the permissive sites in the continuous sequence 20−26, two turns of a regular helix are clearly identified with R1(a)

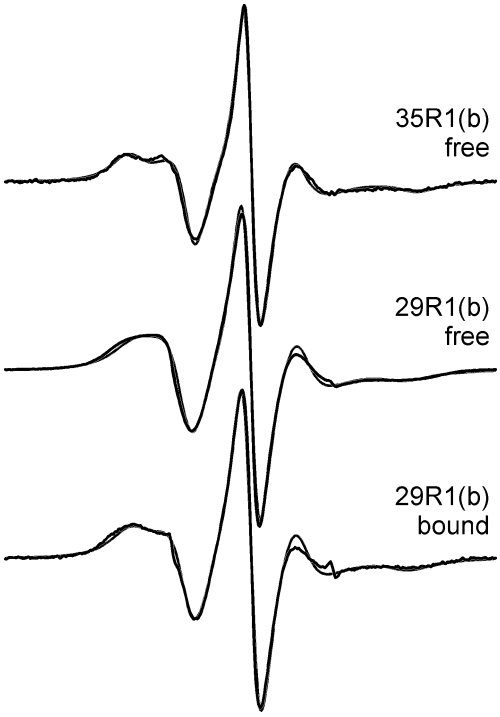

FIGURE 16: Theoretical fits to EPR spectra of R1(b). Experimental spectra (black) and theoretical fits (gray) to the MOMD model for R1(b) at the indicated sites in the free and 2AP-1-bound states.

by a much greater depth of modulation of M_s than for unbound GCN4−58 (Figure 11). The data are in excellent agreement with the orientation of this segment predicted by the crystal structure of the complex (*18*, *19*). In addition, strong spin−spin interaction is observed between residues at site 23 in the pure spin-labeled homodimer, as would be predicted by their proximity in the crystal structure.

Upon binding to the 2AP-1 DNA substrate, M_s drops sharply at sites throughout the basic region, but not in the leucine zipper, indicating that backbone dynamic modes are damped in the binding domain (Figures 11 and 15). Remarkably, a gradient of mobility is retained through the DNA-binding region, indicating significant internal flexibility of parts of the helical "fingers" even when bound to substrate.

In the DNA-bound state, motions are sufficiently damped that the nitroxide residual anisotropies are not completely averaged, and fits to the spectra require $S_{20} > 0$. As shown in Figure 14A, the rates of motion determined from the fits (τ^{-1}) agree rather well with M_s. The order parameters, shown in Figure 14B, rise steadily from the N-terminus to the DNA-binding sites, where the order is a maximum (sites 17 and 18). The order parameter is relatively constant through the leucine zipper but drops significantly from sites 39 to 46, suggesting some "fraying" near the end of the coiled coil. In the crystal structure, a gradient in C^α *B*-factors consistent with the M_s gradient is observed from the N-terminus to residue 17 and from residue 49 to the C-terminus.

The EPR line shapes obtained from MOMD fits for the solvent-exposed helical sites in the bound state also directly reveal the gradient in mobility in the DNA-binding region (Figure 13). Within the basic region, the regular increase in central line width (peak to peak) from 7R1(a) to 17R1(a) reflects a decrease in rate. The apparent increase in width of the *low-field* resonance line from 7R1(a) to 10R1(a) reflects an increased separation of unresolved $A_{||}$ and $A_\perp$

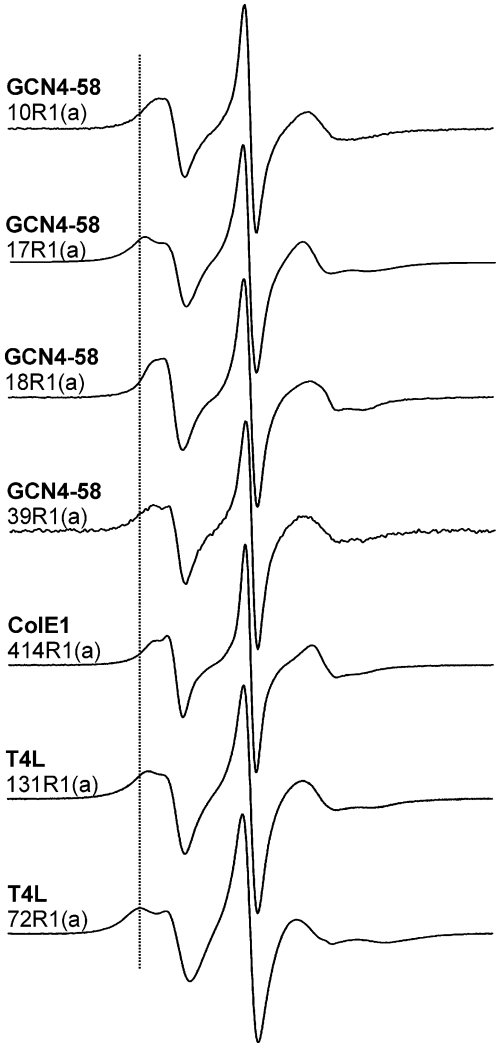

FIGURE 17: Comparison of EPR spectra of R1(a) at solvent-exposed helical sites in GCN4−58 and other proteins. EPR spectra of R1(a) on solvent-exposed helical sites of GCN4−58 bound to 2AP-1 (GCN4−58 10, 17, and 18), colicin E1 (ColE1 414), T4L72, and T4L131. The spectrum shown for GCN4−58 17R1(a) is the most mobile component obtained from fitting. The gray vertical line is drawn as a reference to guide the eye for comparison.

hyperfine extrema due to an increase in S_{20}. Only at 17R1(a) is the order sufficiently high to resolve the two components. The spectrum of 18R1(a) cannot be directly compared because of the unusual anisotropic motion at this site. Within the leucine zipper region, the spectra of 25−43 are relatively similar, reflecting the similar degrees of order. However, the alternation of central line widths in the region 29−46 that reflects the mobility alternation of Figure 14 is evident, as is the high mobility of 46R1(a).

Residue 29R1(b) affords an opportunity to compare the order parameters in the leucine zipper region in the free and bound states. The spectra for the bound and unbound states of 29R1(b) and the corresponding fits are shown in Figure 16. In solution, 29R1(b) has $\tau = 3.4$ ns and $S_{20} = 0.28$. The fit to the same residue, when bound to DNA, gives $\tau = 3.4$ ns and $S_{20} = 0.33$. Thus, there is only a slight increase in order at the beginning of the zipper domain due to DNA binding.

Comparison of GCN4−58 to Other Proteins. Figure 17 compares EPR spectra for R1(a) at helix surface sites in GCN4−58 bound to DNA (10, 17, 18, 39) with similar sites in other helical proteins. The spectrum of 17R1(a) has two components, but the minor component (36%) has a very different mobility. For ease of comparison, the spectrum shown is that for the major component obtained from the best fit. As is evident, GCN4−58 17R1(a) has a spectrum very similar to the "reference" site T4L 72R1(a) and has a similar rate ($\tau = 1.7$ ns) with slightly lower order ($S_{20} = 0.4$). Thus, the backbone at this site, on the outside of the helix directly opposite the DNA contact site, is highly ordered. The adjacent residue 18R1(a) has a similar rate and order parameter, although as mentioned above it has a more complex motion. These two residues represent the most highly ordered sites in the molecule. It is somewhat surprising that R1(a) at sites within the leucine zipper does not have an equally high order parameter, particularly since the S_{NH} order parameters from NMR relaxation data are high throughout this region. This could be due to axial twisting modes of the zipper originating at a flexible region between the DNA-binding site and the zipper. Such motions would constitute rigid body axial rocking motions of the helices and produce effective averaging of the EPR spectral parameters but would have little effect on ^{15}N relaxation.

SUMMARY AND CONCLUSIONS

Collectively, the results presented above indicate that the sequence-dependent rates of motion of the R1(a) side chain at noninteracting helix surface sites reflect backbone dynamics in GCN4−58 on the nanosecond time scale. The rates of these motions can be quantified by the mean rotational diffusion coefficient, as determined by spectral fitting, or by the dimensionless spectral parameter M_s derived from the central line width. In cases where the motional amplitudes are not too large, spectral fitting can also provide an approximate order parameter for the motion, expressed as S_{20}. In this case, an effective order parameter for the backbone motion can be obtained within the context of a simple site-independent model for the internal motion of the R1(a) side chain.

When the amplitudes of R1(a) motion are sufficiently large to extensively average the nitroxide magnetic parameters, S_{20} cannot be determined. In some cases, this problem can be overcome by the use of side chains with hindered internal motions, such as R1(b). The R1(b) side chain has a more highly ordered internal motion, resulting in an increase in the dynamic range for detecting backbone fluctuations.

SDSL mapping of backbone dynamics in GCN4−58 bound to DNA revealed a dramatic damping of backbone fluctuations in the basic region, although a gradient in both rate and order was still detected. Relatively smaller changes were found in the leucine zipper region. The GCN4−58 residues located directly at the DNA-binding site are nearly as rigid as helical sites in globular proteins.

The detection of backbone motions by SDSL as described above is indirect, coupled through the internal motion of the side chain. Nevertheless, the method has distinct advantages over other methods, including relative simplicity of instrumentation, small sample requirements (picomoles of protein), experimental ease (time scale of weeks to prepare a set of mutants in a given sequence), and general applicability to soluble proteins of unlimited molecular mass and membrane proteins.

ACKNOWLEDGMENT

We thank Dr. Arthur G. Palmer, III, for the wild-type GCN4-58 plasmid; Dr. Christian Altenbach for EPR analysis software, scientific discussion, and careful review of the manuscript; Shirley Oga and Mark Fleissner for technical assistance; and Dr. Cameron Mura for helpful comments on the manuscript.

SUPPORTING INFORMATION AVAILABLE

Three tables containing fit parameters for GCN4−58, GCN4−58 bound to 2AP-1, and R1(b). This material is available free of charge via the Internet at http://pubs.acs.org.

REFERENCES

1. Carr, P. A., Erickson, H. P., and Palmer, A. G. (1997) Backbone dynamics of homologous fibronectin type III cell adhesion domains from fibronectin and tenascin, *Structure 5*, 949−959.
2. Ishima, R., and Torchia, D. A. (2000) Protein dynamics from NMR, *Nat. Struct. Biol. 7*, 740−743.
3. Zuiderweg, E. R. (2002) Mapping protein−protein interactions in solution by NMR spectroscopy, *Biochemistry 41*, 1−7.
4. Wang, C., Pawley, N. H., and Nicholson, L. K. (2001) The role of backbone motions in ligand binding to the c-Src SH3 domain, *J. Mol. Biol. 313*, 873−887.
5. Stone, M. J., Gupta, S., Snyder, N., and Regan, L. (2001) Comparison of protein backbone entropy and β-sheet stability: NMR-derived dynamics of protein G B1 domain mutants, *J. Am. Chem. Soc. 123*, 185−186.
6. Yang, D., and Kay, L. E. (1996) Contributions to conformational entropy arising from bond vector fluctuations measured from NMR-derived order parameters: application to protein folding, *J. Mol. Biol. 263*, 369−382.
7. Parak, F. G. (2003) Proteins in action: the physics of structural fluctuations and conformational changes, *Curr. Opin. Struct. Biol. 13*, 552−557.
8. Hammes, G. G. (2002) Multiple conformational changes in enzyme catalyasis, *Biochemistry 41*, 8221−8228.
9. Gerstein, M., Lesk, A. M., and Chothia, C. (1994) Structural mechanisms for domain movements in proteins, *Biochemistry 33*, 6739−6749.
10. Hubbell, W. L., Gross, A., Langen, R., and Lietzow, M. A. (1998) Recent advances in site-directed spin labeling of proteins, *Curr. Opin. Struct. Biol. 8*, 649−656.
11. Hubbell, W. L., Cafiso, D. S., and Altenbach, C. (2000) Identifying conformational changes with site-directed spin labeling, *Nat. Struct. Biol. 7*, 735−739.
12. Columbus, L., Kalai, T., Jeko, J., Hideg, K., and Hubbell, W. L. (2001) Molecular motion of spin labeled side chains in α-helices: analysis by variation of side chain structure, *Biochemistry 40*, 3828−3846.
13. Columbus, L., and Hubbell, W. L. (2002) A new spin on protein dynamics, *Trends Biochem. Sci. 27*, 288−295.
14. Budil, D. E., Lee, S., Saxena, S., and Freed, J. H. (1996) Nonlinear-least-squares analysis of slow-motion EPR spectra in one and two dimensions using a modified Levenberg−Marquardt algorithm, *J. Magn. Reson., Ser. A 120*, 155−189.
15. Mchaourab, H. S., Lietzow, M. A., Hideg, K., and Hubbell, W. L. (1996) Motion of spin-labeled side chains in T4 lysozyme. correlation with protein structure and dynamics, *Biochemistry 35*, 7692−7704.
16. Langen, R., Oh, K. J., Cascio, D., and Hubbell, W. L. (2000) Crystal structures of spin labeled T4 lysozyme mutants: implications for the interpretation of EPR spectra in terms of structure, *Biochemistry 39*, 8396−8405.
17. Bracken, C., Carr, P. A., Cavanagh, J., and Palmer, A. G. (1999) Temperature dependence of intramolecular dynamics of the basic leucine zipper of GCN4: implications for the entropy of association with DNA, *J. Mol. Biol. 285*, 2133−2146.
18. Ellenberger, T. E., Brandl, C. J., Struhl, K., and Harrison, S. C. (1992) The GCN4 basic region leucine zipper binds DNA as a dimer of uninterrupted alpha helices: crystal structure of the protein-DNA complex, *Cell 71*, 1223−1237.
19. Keller, W., Konig, P., and Richmond, T. J. (1995) Crystal structure of a bZIP/DNA complex at 2.2 A: determinants of DNA specific recognition, *J. Mol. Biol. 254*, 657−667.
20. Barbato, G., Ikura, M., Kay, L. E., Pastor, R. W., and Bax, A. (1992) Backbone dynamics of calmodulin studied by ^{15}N relaxation using inverse detected two-dimensional NMR spectroscopy: the central helix is flexible, *Biochemistry 31*, 5269−5278.
21. Hill, D. E., Hope, I. A., Macke, J. P., and Struhl, K. (1986) Saturation mutagenesis of the yeast his3 regulatory site: requirements for transcriptional induction and for binding by GCN4 activator protein, *Science 234*, 451−457.
22. Weiss, M. A., Ellenberger, T., Wobbe, C. R., Lee, J. P., Harrison, S. C., and Struhl, K. (1990) Folding transition in the DNA-binding domain of GCN4 on specific binding to DNA, *Nature 347*, 575−578.
23. Hubbell, W. H., Froncisz, W., and Hyde, J. S. (1987) Continuous and stopped flow EPR Spectrometer based on a loop gap resonator, *Rev. Sci. Instrum. 58*, 1879−1886.
24. Langen, R., Cai, K., Altenbach, C., Khorana, H. G., and Hubbell, W. L. (1999) Structural features of the C-terminal domain of bovine rhodopsin: a site-directed spin-labeling study, *Biochemistry 38*, 7918−7924.
25. Bales, B. L. (1989) Inhomogenously broadened spin-label spectra, in *Biological Magnetic Resonance: Spin Labeling Theory and Applications* (Berliner, L. J., and Reuben, J., Eds.) pp 77−126, Plenum Press, New York.
26. Robinson, B. H., Mailer, C., and Reese, A. W. (1999) Linewidth analysis of spin labels in liquids I. theory and data analysis, *J. Magn. Reson. 138*, 199−209.
27. Stone, T. J., Buckman, T., Nordio, P. L., and McConnell, H. M. (1965) Spin-labeled biomolecules, *Proc. Natl. Acad. Sci. U.S.A. 54*, 1010−1017.
28. Freed, J. H. (1976) Theory of slow tumbling ESR spectra for nitroxides, in *Spin Labeling Theory and Applications* (Berliner, L. J., Ed.) pp 53−132, Academic Press, New York.
29. Alber, T. (1993) How GCN4 binds DNA, *Curr. Opin. Struct. Biol. 3*, 182−184.
30. Altenbach, C., Oh, K. J., Trabanino, R. J., Hideg, K., and Hubbell, W. H. (2001) Estimation of interresidue distances in spin labeled proteins at physiological temperatures: experimental strategies and practical limitations, *Biochemistry 40*, 15471−15482.
31. Mchaourab, H. S., Oh, K. J., Fang, C. J., and Hubbell, W. L. (1997) Conformation of T4 lysozyme in solution. hinge-bending motion and the substrate-induced conformational transition studied by site-directed spin labeling, *Biochemistry 36*, 307−316.
32. Barnes, J. P., Liang, Z., McHaourab, H. S., Freed, J. H., and Hubbell, W. L. (1999) A multifrequency electron spin resonance study of T4 lysozyme dynamics, *Biophys. J. 76*, 3298−3306.
33. Saudek, V., Pasley, H. S., Gibson, T., Gausepohl, H., Frank, R., and Pastore, A. (1991) Solution structure of the basic region from the transcriptional activator GCN4, *Biochemistry 30*, 1310−1317.
34. Saudek, V., Pastore, A., Morelli, M. A., Frank, R., Gausepohl, H., and Gibson, T. (1991) The solution structure of a leucine-zipper motif peptide, *Protein Eng. 4*, 519−529.
35. Griffith, O. H., and Jost, P. C. (1976) Lipid spin labels in biological membranes, in *Spin Labeling Theory and Applications* (Berliner, L. J., Ed.) pp 454−523, Academic Press, New York.

BI0497906